JOURNAL OF PROPULSION AND POWER
Vol. 21, No. 4, July–August 2005

Improved Confinement in Inertial Electrostatic Confinement for Fusion Space Power Reactors

T. J. McGuire* and R. J. Sedwick†
Massachusetts Institute of Technology, Cambridge, Massachusetts 02139

Multiple improvements to the inertial-electrostatic-confinement (IEC) fusion concept are presented. Prior efforts have consisted of considerable theoretical effort and numerous ground experiments resulting in the fusion of D-D, D-T, and D-^{3}He at rates on the order of 10^{10} reactions per second. Theory developed in the paper shows that prior experiments, which observed a linear relationship between reaction rate and background pressure, were "confinement" limited. With improved ion confinement, the reaction rate and the pressure should decouple at high pressure where the beam-beam reactions are not yet dominant. Highly efficient beam-beam reaction rates are found to dominate the total reaction rate as ion lifetime is increased. The ion lifetime is limited mainly by collisions with background particles and by defocusing. The naturally low background pressure available in the space environment effectively eliminates background pressure as a constraint on ion lifetime, leaving defocusing as the main ion lifetime limiter. To improve ion confinement, multiple grids are introduced to produce focusing channels for ions. The other main loss mechanism is electrons streaming from the core region to the anode. An additional grid is placed within the cathode, providing a central trap for core electrons. Theory predicts that improvements in confinement should be verifiable using existing relatively high-pressure ground systems and the proposed experiment design is presented. The buildup of space charge in the focusing lenses is used to estimate improvements in confinement from < 10 passes to the order of 1000 passes, boosting the performance of IEC reactors by two orders of magnitude, yielding in the near term, a fast neutron source suitable for medical, security, research, and industrial applications. Further increases of confinement will enable net power production in reactors ideally suited for spacecraft power production as a result of low system mass in comparison to magnetic confinement fusion.

Nomenclature

A_c	=	acceptance, ratio of beam radius to beam opening radius
A_g	=	acceptance at a particular grid location
E_{cat}	=	energy to move a singly charged ion to the cathode grid, eV
E_{fusion}	=	energy released by a fusion reaction, eV
E_r	=	space-charge electric field radial to a beam, mks
e	=	electron charge, 1.602×10^{-19}C
F	=	focusing factor, ratio of core radius to beam radius at cathode
i_{fusion}	=	portion of input current that fuses, mks
$i_{\text{in-beam}}$	=	input current per beam, mks
$i_{\text{in-tot}}$	=	total input current, mks
KE_0	=	kinetic energy of a singly charged ion at the center of the device, eV
N	=	number of beams, one beam corresponds to a diameter of the sphere
n	=	number density, mks
n_{beam}	=	beam number density, mks
n_{core}	=	core number density, mks
p_{torr}	=	device background pressure, torr
R_a	=	outermost anode radius, mks
R_{cat}	=	cathode radius, mks
r	=	local radius of ion beam, mks
r_c	=	core radius, mks
r_{cat}	=	beam radius at the cathode grid, mks
$r_{\text{cat-max}}$	=	opening radius in the cathode grid, mks
r_g	=	beam radius at a particular grid, mks
$r_{\text{g-max}}$	=	opening radius at a particular grid, mks
V_{go}	=	central potential increase of a beam caused by space charge
v	=	velocity, mks
v_{core}	=	velocity of ions in the core, mks
v_g	=	velocity at a particular grid location, mks
v_{rel}	=	relative velocity of two fusing particles, mks
x	=	path length, mks
η	=	electrical conversion efficiency
λ	=	wavelength of an instability, mks
σ_a	=	atomic processes cross section, combination of ionization and charge exchange, mks
σ_{fus}	=	fusion cross section, mks
Φ	=	transparency of grids, fraction of area that is open
ω_p	=	plasma frequency, mks
$\#p$	=	average number of passes (diameters) an ion makes through the device
$\%f$	=	percentage of input ions that fuse
$\langle\,\rangle_c$	=	average over core particle distribution, mks
$\langle\,\rangle_p$	=	average over an ion path from anode to core, mks

Presented as Paper 2003-4829 at the AIAA Joint Propulsion Conference, Huntsville, AL, 20–23 June 2003; received 24 February 2004; revision received 20 October 2004; accepted for publication 14 November 2004.

*Graduate Research Assistant, Space Systems Laboratory, 77 Massachusetts Avenue. Member AIAA.

†Principle Research Scientist, Space Systems Laboratory, 77 Massachusetts Avenue. Senior Member AIAA.

Introduction

INERTIAL-ELECTROSTATIC-CONFINEMENT-FUSION (IEC) devices have produced fusion reactions in D-D, D-T, and D-He^3 plasma at rates of up to 10^{10} reactions per second.[1–4] These devices are relatively small, with chamber diameters less than a meter, and the research expenses to date have been on a much smaller scale than magnetic or target fusion. The electrical efficiency of IEC systems is still very low however, with only milliwatts of fusion power produced for tens of kilowatts input electrical power. They are promising for the simplicity of the concept, the controllability of reactions, and the suitability to aneutronic fuels and direct

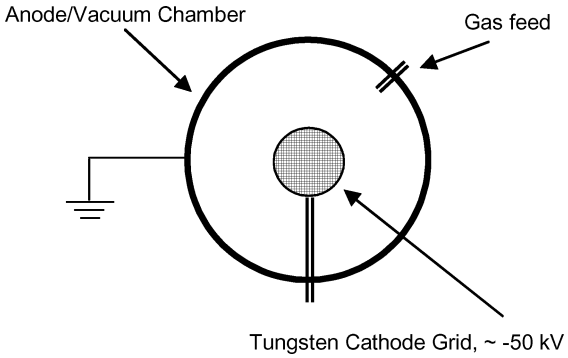

Fig. 1 General IEC device configuration.

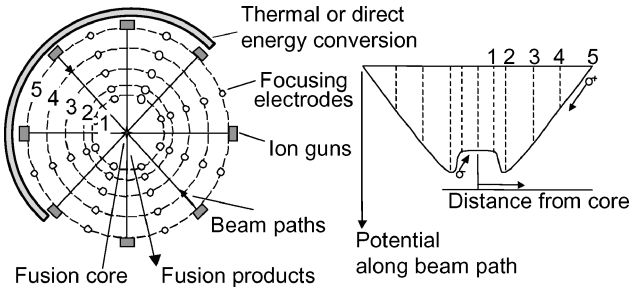

Fig. 2 Multiple grid layout and potential structure along a radial beam path.

energetic conversion.[5] As a spacecraft power and propulsion system, the low mass of electrostatic grids is vastly superior to massive magnetic coils required for tokamaks or magnetic mirror confinement systems. By utilizing aneutronic fuel cycles, the massive shielding required of neutron-producing fission or fusion reactors is not necessary. Also, a significant political advantage over radioisotope thermal generators is the ability to launch a totally nonreactive system.

The general setup of an IEC is shown in Fig. 1. The ions are confined by electric fields supported by low-mass, spherical grids. Laboratory systems have grids welded from stainless and refractory metal wire, and the system is enclosed in a vacuum chamber. A space reactor would most likely have grids constructed of metal tubes that could support coolant, and the system would be open to space vacuum. Ions are created at the anode via a glow discharge, electron impact ionization, or ion guns. The ions then fall into the center of the device. As they converge, fusion occurs between ions colliding with each other and with the background gas. Most of the ions that do not fuse on the first pass move towards the anode and are reflected. Ions then return to the core for another pass, and this process repeats, yielding many opportunities to fuse. Fusion products stream away from the device core and are either collected by a solid-wall thermal-based energy conversion system or a gridded electrostatic energy conversion system, as shown in Fig. 2.

Theory and experiments have suggested that virtual cathodes and anodes can be created at the center of these systems, allowing plasma to be electrostatically trapped in these regions.[2,6] Proponents of this concept are hopeful that these potential structures will allow for favorable, highly nonlinear reaction rate dependencies on input current and input power. However, these structures can be defocusing to the ions, causing buildup of unwanted nonradial velocity. By deriving the reaction-rate scaling, this paper will show the consequences of operating the device without the benefit or hindrance of these structures. Further, theoretical predictions of virtual cathodes and anodes have invoked an idealized spherical symmetry in the device that does not exist in gridded devices. The collection of grids and high-voltage stalks creates asymmetries that do not allow ions to oscillate in the device. These asymmetries can be exploited, however, by using multiple grids to create electrostatic lenses that actually focus the ions instead of causing them to deflect away from radial trajectories. Proposed improvements to the IEC are shown in Fig. 2. Grids (4 and 3) are introduced between the anode (#5) and cathode (2) grids to provide electrostatic focusing of the ion beams.[7] In addition, a decelerating grid is placed inside the cathode in order to create an electron trap (1), preventing electrons from freely streaming from the core to the anode. The ion density buildup at the device center is no longer an unrealistic, idealized collection of shell structures, but it is now the region of overlap from numerous recirculating ion beams. These improvements act to increase the ion lifetime, which from the following derivations of reaction rates is the key to making the device more efficient so as to produce net power.

Reaction Rates

Using a gridded IEC, one can estimate the fusion reaction rate by looking at contributions of beam-background and beam-beam interactions. Contributions caused by energetic neutrals produced from charge-exchange (CX) collisions will be neglected here because they are lost immediately to grids and walls. The ions created by CX collisions are of too low energy to significantly contribute to the reaction rate. The remaining two reaction sources must be integrated over the entire vacuum vessel and are given by

$$\dot{r} = \int_V n_{\text{back}}\, n_{\text{beam}} (\sigma_{\text{fus}} v)_{\text{beam/back}} + \frac{n_{\text{beam}}^2}{4} (\sigma_{\text{fus}} v)_{\text{beam/beam}}\, \mathrm{d}V \quad (1)$$

The problem is then to define the densities throughout the device volume. The background density is a linear function with pressure at a given gas temperature. The bulk gas in an IEC can be assumed to be at room temperature given a low power input and effective cooling of the vacuum vessel to the room temperature. From the ideal-gas law and the pressure given in torr, the background density can be expressed as

$$n_{\text{back}} = 3.218 \times 10^{22} \cdot p_{\text{torr}} \quad (2)$$

The background density is assumed to be uniform throughout the chamber, which neglects the possibility of 'Star' mode microchannels[3] selectively reducing the pressure along the channels. This is shown by calculation of the characteristic mean free path for ionization of the background gas by the accelerated ions. A peak ionization cross section of 2×10^{-20} m^2 and a high estimate of plasma density of 10^{20} m^{-3} gives a mean free path of 0.5 m, which is much larger than characteristic beam and core dimensions in IEC devices.[8] Advanced systems with very high densities and trapped particle populations might, however, modify the uniform background gas distribution, but are not considered in detail here.

The beam density is given by evaluating the ion beam particle flux:

$$n_{\text{beam}} = \frac{i_{\text{in-beam}} \# p}{e v A} = \frac{i_{\text{in-beam}} \# p}{e \sqrt{[2eE_{eV}(x)/m_i]}\, \pi r^2(x)} \quad (3)$$

where the ion thermal energy is assumed to be negligible compared to the kinetic energy acquired from the potential field. This model is made to apply to a system in which ions are not yet confined to the point where thermalization of the ion energy is important. A break-even system would have ion beam thermalization, but current experiments do not yet confine ions long enough for this to occur. The ions are assumed to oscillate an average number of times through the system, and the beams are then populated by the recirculating ions such that the average number of passes multiplies the beam density.

This treatment also assumes that only ions that are traveling along the beam paths and have not undergone a collision are still "confined". Ions that are not traveling on these quasi-radial trajectories caused by collisions have a greatly reduced probability for fusion and are considered to be lost. Treating the average number of passes as a metric for ion confinement is acceptable provided that ion confinement limits the ion lifetime. The ion lifetime can also be limited by other processes such as charge exchange, ionization, and fusion. This will be shown later to be essential in understanding the performance of experiments to date.

The core density can similarly be written as the general beam density evaluated at the core position, but now multiplied by the number of beams that overlap in the core region.

$$n_{\text{core}} = \frac{N i_{\text{in-beam}} \# p}{e\sqrt{(2eE_{\text{eV-core}}/m_i)}\pi r_c^2} \tag{4}$$

Beam-Background Reactions

The beam-background interactions are assumed to involve stationary neutrals, which is valid given that the wall temperature limits the temperature of the neutrals. With low input power, the wall can easily be kept cool. Even at elevated wall and grid temperatures (1000s of K) present in break-even reactors, the neutral velocities are negligible compared to the charged particle velocities (keVs) and can be taken as stationary. Therefore, the relative velocity is given by the ion energy, which is a function of the position in the potential. The same relative velocity defines the fusion cross section. The beam-background contribution is evaluated over the volume of one beam and multiplied by the number of beams, as shown in Eq. (5):

$$\dot{r}_{\text{beam-back}} = 2\pi N \int_0^{R_a} n_{\text{beam}} n_{\text{back}} \sigma_{\text{fus}}(x) v(x) r(x)^2 \, \mathrm{d}x \tag{5}$$

The expressions for density can be substituted, yielding an expression where the dependence on the radius of the beams is eliminated and the spatial dependence is reduced to an integral of the cross section over the path length. The total input current is given by multiplying the input current per beam by the number of beams. Making these substitutions, the result is a linear dependence on input current and background pressure, for a given confinement time (number of passes).

$$\dot{r}_{\text{beam-back}} = \left(i_{\text{in-tot}} \# p \cdot 6.436 \times 10^{22} \cdot p_{\text{torr}}\right) \Big/ e \int_0^{R_a} \sigma_{\text{fus}}(x) \, \mathrm{d}x \tag{6}$$

The spatial dependence can be further simplified by assuming that the cross section for fusion is negligible outside the cathode grid as a result of the $\sim 1/r$ potential rise and quickly reduced energy of the ions. If the incoming ion beams are neutralized as they enter the cathode, they will drift through the center region with constant velocity, assuming that the core electrons are cool enough as to not create a potential well. Thus, the velocity and fusion cross section will be constant within the cathode of the device. Under these assumptions, the beam-background reaction rate is given by

$$\dot{r}_{\text{beam-back}} = \left[\left(i_{\text{in-tot}} \# p \cdot 6.436 \times 10^{22} \cdot p_{\text{torr}}\right) \Big/ e\right] \sigma_{\text{fus}}(KE_0) R_{\text{cat}} \tag{7}$$

In Fig. 3, the fusion cross sections for a few of the reactions of interest are given.[9] Equation (7) is strictly valid for only a single species reaction such as D-D. Corrections for multiple species can be found by summing the interactions of each species with all of the others.

Beam-Beam Reaction in the Device Core

The beam-beam interaction can be divided into two parts: 1) in the dense core and 2) in the "spokes" formed by the counterstreaming beams, as shown in Fig. 4. The dense core can be modeled as a region of overlap of many converging beams, each with a specific radius. Given the long mean free paths for fusion and ion-ion scattering cross sections at fusion relevant energies (greater than 25 keV), the beams will only weakly couple via collisions. A quick estimate of the ion-ion collision mean free path can be taken by using the standard expression for thermal ion-ion collision frequency. Using high estimates of deuterium ion density of 10^{20} m^{-3}, energy and temperature equal to 25 keV and a coulomb logarithm of 15 yields a mean free path for ion-ion collisions of 5×10^5 m. For a characteristic device diameter of 0.5 m, this equals one million passes. Fusion mean free paths can be estimated with a density of 10^{20} m^{-3} and a peak cross section of 1 barn (10^{-28} m^{-2}), yielding

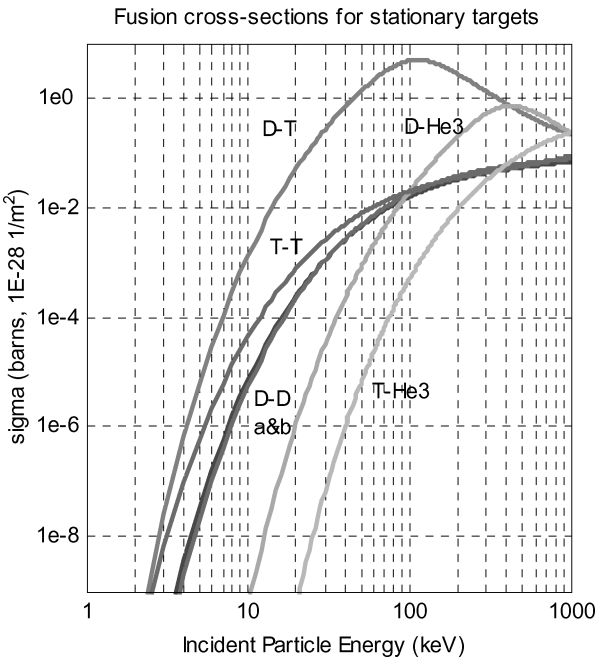

Fig. 3 Target fusion cross sections as a function of incident particle kinetic energy.[9]

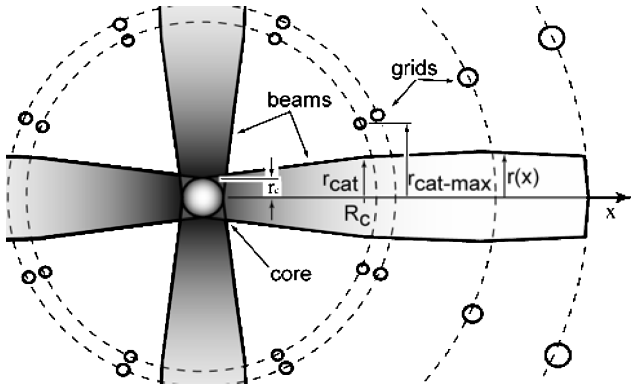

Fig. 4 Model of two crossing ion beams and core size as a result of beam compression.

10^8 m or 200 million passes through our characteristic device. Current state-of-the-art confinement is well below these levels, in the 10-pass area, and this paper deals with the effect of increasing that to 1000 to 10,000 passes. Because this model looks to explain and extend the current state of the art, not exactly describe a break-even system, the ion-ion collisions can be taken to be a weak interaction mechanism.

The other method of ion interaction would be space-charge structures. In a device with no neutralization, the incoming ions will tend to produce significant regions of space charge, producing the alternating virtual anodes and cathodes called "poissors" as predicted by Farnsworth[10] and observed in numerous experimental efforts.[6] In the current effort to reduce the defocusing effects of these space-charge structures, an electron cloud is trapped within the cathode grid in order to neutralize the incoming ion beams. This innovation should greatly reduce the buildup of space charge at the device core and allow the core regions to be simply modeled as a region of beam overlap. The overall applicability of this model to prior experiments is still good because no prior IEC experiments have found evidence of significant beam-beam fusion reactions, so that most of the important relations for prior work reside in the beam-background term. Given a sufficient number of constant density profile beams, the core is well modeled as a uniform density region with spherical boundary

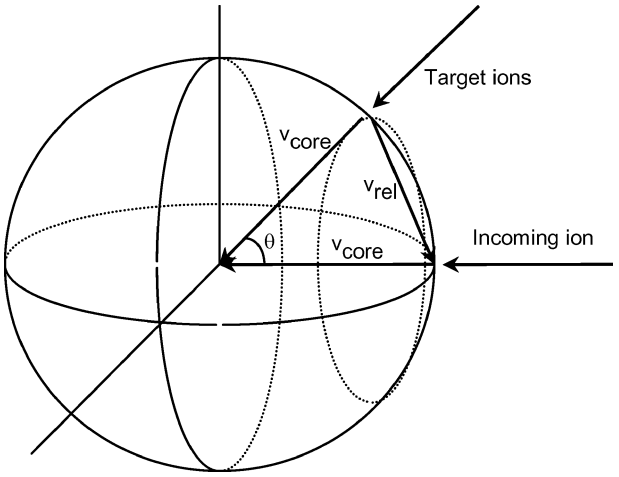

Fig. 5 Diagram of collisions in a uniform core, for averaging over core population.

of radius. The total fusion reaction rate in the core volume is given by

$$\dot{r}_{\text{beam-core}} = \tfrac{4}{3}\pi r_c^3 \cdot \left(n_{\text{core}}^2/4\right)\langle\sigma_{\text{fus}} v\rangle_c \tag{8}$$

Substitute the core density Eq. (4) into Eq. (8) and simplify:

$$\dot{r}_{\text{beam-core}} = \frac{i_{\text{in-tot}}^2 \#p^2}{3\pi e^2 r_c v_c^2}\langle\sigma_{\text{fus}} v\rangle_c \tag{9}$$

In the core, the fusion cross section must be averaged over an isotropic velocity distribution because the relative velocity of ions varies from head-on to glancing collisions. This value is given by averaging over all of the target ions, which are spread uniformly over a sphere in velocity space, as shown in Fig. 5.

$$\langle\sigma_{\text{fus}} v\rangle = \frac{1}{SA}\int \sigma v \,\mathrm{d}A = \frac{1}{4\pi v_{\text{core}}^2}\int_0^\pi \sigma(v_{\text{rel}}) v_{\text{rel}}\, 2\pi v_c^2 \sin\theta \,\mathrm{d}\theta$$

$$v_{\text{rel}} = 2v_{\text{core}}\sin\left(\frac{\theta}{2}\right)$$

$$\langle\sigma_{\text{fus}} v\rangle = v_{\text{core}}\int_0^\pi \sigma\left[2v_{\text{core}}\sin\left(\frac{\theta}{2}\right)\right]\sin\left(\frac{\theta}{2}\right)\sin\theta\,\mathrm{d}\theta$$

$$= v_{\text{core}}\int_0^\pi \sigma\left[4KE_0\sin^2\left(\frac{\theta}{2}\right)\right]\sin\left(\frac{\theta}{2}\right)\sin\theta\,\mathrm{d}\theta \tag{10}$$

where the fusion cross section can be evaluated with either the core velocity or energy. This treatment is only valid for single species reactions such as D-D as shown in Fig. 6, but can be similarly derived for species of different charge and mass.

Beam-Beam Reactions Outside of the Core

The beam-beam contribution from the spokes is found by integrating over the volume of a given spoke:

$$\dot{r}_{\text{beam-spokes}} = 2N\int_{r_c}^{R_a}\int_S \frac{n_{\text{beam}}^2}{4}\langle\sigma_{\text{fus}}(x) v(x)\rangle_{\text{beam-beam}}\,\mathrm{d}A\,\mathrm{d}x$$

$$= 2\pi N\int_{r_c}^{R_a}\frac{n_{\text{beam}}^2}{4}\sigma_{\text{fus}}[2v(x)]\,2v(x)r(x)^2\,\mathrm{d}x \tag{11}$$

where the beams are assumed to collide head on with the relative velocity of a collision given by twice the single particle's velocity at that position x along the path. This is valid for the nonrelativistic acceleration of ions where a characteristic ion speed is $\sim 2\times 10^6$ m/s for deuterium at a kinetic energy of 50 keV. In the regime of a low number of passes, the ion velocity can be assumed to be only

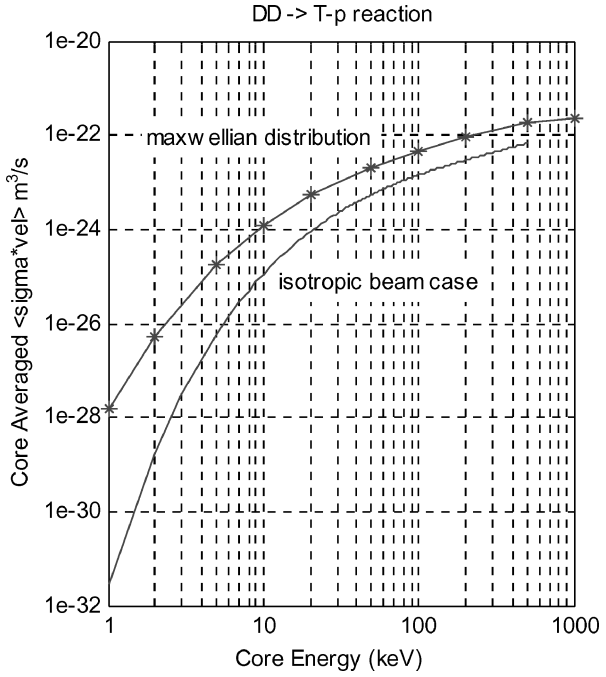

Fig. 6 Core-averaged product of cross section and relative velocity for D-D reaction over a range of core ion kinetic energies.

a function of the potential field and thus the path. Similarly, the cross section can be evaluated at a given position with the relative velocity at that location. Here again, these simplifications would break down for ions undergoing enough passes so as to experience a few ion-ion scattering events and thereby lose energy and possibly gain significant nonradial velocity components, causing the ions to be no longer "in" the beam. Also, the beam is assumed to possess a constant density profile and have a beam radius that varies with distance from the center of the sphere x. Then substitute for the beam density, Eq. (3), and simplify

$$\dot{r}_{\text{beam-spokes}} = \frac{N i_{\text{in-beam}}^2 \#p^2}{\pi e^2}\int_{r_c}^{R_a}\frac{\sigma_{\text{fus}}(x)}{v(x)r(x)^2}\,\mathrm{d}x \tag{12}$$

Notice that the region immediately outside of the cathode can contribute to the fusion rate because ions are counterstreaming there at high velocity, at essentially the same fusion conditions as immediately inside the cathode grid. Despite this fact, the rate quickly drops off as the potential outside the cathode rises, and, for clarity, this region of fusion production will be ignored here as a conservative estimate. The upper limit of the integral in Eq. (12) then becomes the cathode radius.

The effect of beam compression can be captured by considering the beam radius to be a linear function of axial beam position inside the cathode as shown in Fig. 3. Beam compression or expansion could be produced by focusing properties of the electrodes and the space charge of the beam, with the beam shaped as in a linear accelerator. The beam radius can then be written as

$$r(x) = r_c + [(r_{\text{cat}} - r_c)/R_{\text{cat}}]x \tag{13}$$

Then let the beam radial focusing factor be the ratio of the beam radius at the cathode grid to the beam radius at the device center.

$$F = r_{\text{cat}}/r_c \tag{14}$$

If the region within the cathode is assumed to be at constant potential, the ions will drift through this region. This situation is assumed for ion beams that are adequately neutralized by an electron source within the cathode grid. A trapping potential difference exists on the cathode grids (grids 1 and 2 in Fig. 2): first to contain streaming electrons and prevent them from being lost to the anode wall or grid,[1] and second to confine a near-thermal neutralizing

population of electrons. The neutralizing ability of these electrons is an ongoing area of research, with similarities to the neutralizers in Kaufman-type ion engines. This model for beam-beam interactions would not be strictly valid for most prior IEC devices because potential structures are allowed to develop within the cathodes as a result of charge imbalance and electrons were freely lost to the anode. As long as the trapped electron population remains near the grid temperature at standard densities (10^{15} to 10^{20} m^{-3}), the potential produced by this cloud will not have a significant impact on the ion velocities within the cathode. In advanced devices, especially those without grids, a trapped electron cloud that has gained significant temperature caused by ion heating could be made to produce its own confining well, with more complex ion dynamics. The drifting ion assumption thus allows the velocity and cross section to be taken outside the integral as constants. By substituting Eq. (13) into Eq. (12) and simplifying, the beam-beam fusion rate in the spokes can be written as

$$\dot{r}_{\text{beam-spokes}} = \frac{i_{\text{in-tot}}^2 \#p^2 \sigma_{\text{fus}}(4KE_0)}{\pi e^2 N v_{\text{core}}} \int_{r_c}^{R_c} \frac{1}{\left\{r_c + [(r_{\text{cat}} - r_c)/R_{\text{cat}}]x\right\}^2}\,\mathrm{d}x$$

$$\dot{r}_{\text{beam-spokes}} = \frac{i_{\text{in-tot}}^2 \#p^2 \sigma_{\text{fus}}(4KE_0)}{\pi e^2 N v_{\text{core}}} \frac{1}{r_c r_{\text{cat}}} \frac{R_{\text{cat}} - r_c}{1 + (r_{\text{cat}} - r_c)/R_{\text{cat}}} \tag{15}$$

Substitute in Eq. (14) for the focusing factor, Eq. (14):

$$\dot{r}_{\text{beam-spokes}} = \frac{i_{\text{in-tot}}^2 \#p^2}{\pi e^2 v_{\text{core}}} \frac{\sigma_{\text{fus}}(4KE_0)}{N r_{\text{cat}}} \frac{R_{\text{cat}}}{r_c} \frac{1 - r_{\text{cat}}/R_{\text{cat}} F}{1 + (r_{\text{cat}}/R_{\text{cat}})(1 - 1/F)} \tag{16}$$

If many beams are used ($N \gg 1$), the number of beams and the cathode radius can be related to the maximum beam radius at the cathode by writing a ratio of surface areas. Also, let the acceptance be the ratio between the beam radius and the beam opening radius.

$$r_{\text{cat-max}} = R_{\text{cat}} \sqrt{2\Phi/N}, \qquad r_{\text{cat}} = A_c\, r_{\text{cat-max}} \tag{17}$$

where Φ is calculated to be $\sim$91.7% for a hexagonal packing of circles on a plane and the noncircle area taken to be the grid. Greater transparencies are possible for noncircular beam openings, for example, constructed of thin wires or tubes forming polygonal facets on a sphere. By substituting these relations into Eq. (16), assembling and simplifying the complete reaction caused by all of the rate components, Eqs. (16), (10), and (7), the total rate is

$$\dot{r} = \frac{i_{\text{in-tot}} \#p \cdot 6.436 \times 10^{22} \cdot p_{\text{torr}}}{e} \sigma_{\text{fus}}(KE_0) R_{\text{cat}} + \frac{i_{\text{in-tot}}^2 \#p^2}{\pi e^2 v_{\text{core}}} \frac{1}{R_{\text{cat}} A_c \sqrt{2\Phi}} \left[\frac{\langle \sigma_{\text{fus}} v \rangle}{3 v_{\text{core}}} F \sqrt{N} + \frac{\sigma_{\text{fus}}(4KE_0)}{A_c \sqrt{2\Phi}} \frac{1 - (A_c/F)\sqrt{2\Phi/N}}{1 + A_c \sqrt{2\Phi/N}\,(1 - 1/F)} \right] \tag{18}$$

The first term in Eq. (18) is the reaction rate caused by beam-background interactions. The second term in the equation shows the combined beam-beam reaction rate as a result of beam-core and beam-spoke interactions, respectively. Notice that only the core beam-beam rate term scales strongly with the focusing factor, whereas the beam-background and spoke contributions are unaffected by focusing. Also, the core has a fairly important square-root dependence on the number of beams, but the spokes are only weakly dependent on the number of beams. The input current and confinement for the beam-beam term have a quadratic dependence. This strong scaling has been the historical impetus for high current pulsed experiments, as it is hoped that the fusion rate will increase faster than the ion losses with favorable scaling laws. As for geometry, the beam-background term scales linearly with the device size, specifically the cathode radius. The beam-beam terms however can be rewritten to show that the key geometrical scaling is an inverse relation to core size. For a given focusing factor, the beam-beam reaction rate is then inversely related to cathode radius. This would suggest that if focusing cannot be easily controlled it would be easier to produce highly reactive cores in smaller devices.

Relative Importance of Beam-Background to Beam-Beam Reactions

The ratio of beam-background fusion reactions to beam-beam fusion reactions can be calculated:

$$\frac{\dot{r}_{\text{beam-back}}}{\dot{r}_{\text{beam-beam}}} = 6.436 \times 10^{22} \cdot p_{\text{torr}} \pi e R_{\text{cat}}^2 v_{\text{core}} A_c \sqrt{2\Phi} \Bigg/ \left\{ i_{\text{in-tot}} \#p \cdot F \left[\frac{\langle \sigma_{\text{fus}} v \rangle}{\sigma_{\text{fus}}(KE_0)} \frac{\sqrt{N}}{3 v_{\text{core}}} + \frac{\sigma_{\text{fus}}(4KE_0)}{\sigma_{\text{fus}}(KE_0)} \frac{1}{A_c \sqrt{2\Phi}} \times \frac{1 - (A_c/F)\sqrt{2\Phi/N}}{1 + A_c \sqrt{2\Phi/N}\,(1 - 1/F)} \right] \right\} \tag{19}$$

For the favorable beam-beam reaction scaling to dominate the reaction rate, this ratio must be less than one. This condition is met by decreasing the operating pressure, making the device smaller, increasing the input current, increasing the ion confinement, and increasing the focusing F. The ratio is a weaker function of the cathode potential and number of beams. Although this suggests that high-power, pulsed experiments might be a viable way to explore the beam-beam scaling, the ion confinement term will be shown later in this paper to be inversely dependent on the input current when the space charge of the beams becomes important. To examine beam-beam interactions while avoiding this limiting mechanism, it seems favorable instead to operate at lower pressures with better confinement.

Distribution of Beam-Beam Fusion Rates

The distribution of beam-beam fusion reactions between fusion in the core and the spokes can be found by looking at the ratio of these two terms.

$$\frac{\dot{r}_{\text{beam-core}}}{\dot{r}_{\text{beam-spokes}}} = \frac{\langle \sigma_f v \rangle}{v_c \sigma_f(4KE_0)} \frac{\sqrt{N} A_c \sqrt{2\Phi}}{3} \times \frac{1 + A_c \sqrt{2\Phi/N}(1 - 1/F)}{1 - (A_c/F)\sqrt{2\Phi/N}} \tag{20}$$

This ratio describes the relative reactivity of the core and how well the device approximates a point source. When expressing the right-hand side as a product of three fractions, the first and third fractions in the preceding expression are of order one, and the most important variable in the second fraction is the square root of the number of beams. When the number of beams is low, as on many experiments to date, the beam-beam fusion rate is spread out over the cathode volume. However, this effect was not observed in prior experiments to date because the background rate swamped any signal from the beam-beam fusion rate. As N gets large, the beam-beam fusion is more localized to the core, which should be generally desirable for designing low-loss energy conversion systems where streaming reaction products are least likely to impact grids before exiting the semitransparent system.

Break-Even Operation

Working from the reaction-rate expressions, there appear to be two main methods to increase the fusion rate: 1) a large system geared towards beam-background operation and 2) a small, low-pressure system geared towards beam-beam reactions. The system gain, the ratio of fusion energy produced to input energy Q will be the deciding factor between these two approaches. It will be shown that the confinement time for this model is the key variable for determining the system gain and that only the low-pressure system will lead to a viable, high Q device.

The two main loss mechanisms for a gridded IEC are ions impacting the cathode grids and electrons streaming to the anode grids.

Ions impacting the cathode act to raise the potential of that grid, and some energy must be expended to remove that ion's charge and maintain the potential on that grid. Also, the impacting ions can cause the emission of secondary electrons, which are then lost to the anode. Although the secondary emission of electrons has been an important loss mechanism in IEC experiments to date, the electron trapping grids used in this concept are assumed to eliminate the electron streaming loss. This effect was experimentally observed in Hirsch's work, in which a secondary cathode grid biased to a potential on the order of 1 kV effectively halted the streaming electron current.[1] Many different mechanisms deviate the ions from purely radial paths and cause them to impact the cathode grid. These include tangential forces from the grids themselves, tangential forces from the ion beam space charge, ionization and charge exchange with the background neutrals, high-angle scattering collisions with other ions, ion thermalization within the beams, and direct impact of ions unfortunate enough to be produced on a path leading directly to a grid. A simple expression for the gain can be written looking at the frequencies and associated energy losses for these mechanisms in comparison to the fusion reactions, assuming the electron loss can be effectively halted by the trapping grids.

$$Q = P_{\text{elec}}/P_{\text{in}} = (\eta E_{\text{fusion}}/E_{\text{cat}})[\dot{r}_{\text{fusion}}/(i_{\text{in-tot}}/e - i_{\text{fusion}}/e)] \quad (21)$$

where the fraction of input current that fuses is related by

$$i_{\text{fusion}}/e = 2\dot{r}_{\text{fusion}} = \%f \times i_{\text{in-tot}}/e \quad (22)$$

Solve for the percentage that fuse:

$$\%f = 1/[(1/2Q)\eta(E_{\text{fusion}}/E_{\text{cat}}) + 1] \simeq (E_{\text{cat}}/E_{\text{fusion}})(2Q/\eta) \quad \text{for} \quad Q \le 10 \quad (23)$$

Table 1 shows the calculation of the fraction of ions that must fuse to maintain $Q = 1$ and $Q = 5$ for various fusion fuels, given an electrical conversion efficiency of 35%. The value of $\eta = 0.35$ is assumed here in all cases, although this value could be as high as 0.85 for direct electrical conversion of aneutronic fuels.

The conditions for $Q = 1$ and $Q = 5$ are calculated because a working system would need a gain considerably greater than one to account for overall system inefficiencies. These fractions range from 1 to 50%, indicating that the fusion timescale must be similar to, if not less than the loss timescales. In other words, if half of the input ions are to fuse, the timescale for fusion should be equal to the timescale for the loss routes. The limiting number of passes through the device can be found for each process in the system, including fusion, high angle ion scattering, and atomic processes such as charge exchange, ionization, and recombination. Simple collision cross-section models give these timescales as

$$\tau = 1/n\sigma v, \qquad \#p = 1 \Big/ 2\int_0^{R_a} n_{\text{targets}}\sigma \, \mathrm{d}x \quad (24)$$

As a conservative approximation, the atomic processes can be assumed to cause irreparable damage to a candidate ion, rendering it unable to fuse by disrupting its energy and/or trajectory. In reality, some nonfusion reactions will act to gradually reduce the energy of an ion. The atomic processes then severely limit the lifetime of an ion as a result of the huge difference in cross sections between fusion and atomic processes and the high background pressure in most of the experiments to date. The ratio of the fusion and atomic timescales is then given by

$$\tau_{\text{fusion}}/\tau_a = (R_a/r_c)(\sigma_a/\sigma_{\text{fusion}})(n_{\text{back}}/n_{\text{core}}) \quad (25)$$

where the geometrical scaling occurs because the majority of fusion reactions are occurring in the dense core r_c and atomic processes occur throughout the device volume R_a. For this ratio to be less than one, core number density must outweigh the background density by the combined factors of geometry and cross section. Even under these conservative approximations, for the fusion to dominate the core density should be $\sim$10 orders higher than the background. All IEC experiments to date have used operating pressures greater than 10^{-5} torr and have not operated near this state.[1,3,11] This also shows that increasing the beam-background reactions is not a viable way to increase Q because it relies on a high background density to achieve significant fusion output. To determine if beam-beam operation is viable, the prominent mechanisms limiting confinement are examined.

Table 1 Required ion fusion rates for various fuels, $\eta = 0.35$

Fuel	E_{fusion}, MeV	E_{ion}, keV	%f, $Q = 1$	%f, $Q = 5$
D-T	17.6	50	0.0160	0.0751
D-D	3.65	100	0.1354	0.439
D-He^3	18.3	100	0.0303	0.135

Pressure Limited Ion Confinement

Recognizing that the atomic processes will often be the limiting factor for ion lifetime in experiments with relatively high background pressure, the number of passes can be expressed as a path-averaged expression of the atomic cross sections and density in terms of pressure:

$$\#p = 1 \Big/ 2n_{\text{back}}\int_0^{R_a} \sigma_a(x)\,\mathrm{d}x = 1/2n_{\text{back}}R_a\langle\sigma_a\rangle_p = 1\Big/\left(6.436\times10^{22}R_a p_{\text{torr}}\langle\sigma_a\rangle_p\right) \quad (26)$$

The atomic cross sections for deuterium will be nearly identical to those of hydrogen, plotted in Fig. 7. At thermal energies the cross section is about $5e{-}19\ \text{m}^2$ and is dominated by charge exchange. As fusion energies are achieved, ionization becomes more important, and the cross section is reduced to about $1e{-}20\ \text{m}^2$. The path average of the cross section depends on the velocities caused by the specific device potential profile. The potential profile will be assumed to be constant (as shown in Fig. 2) inside the cathode and approximated as $1/r$ between the anode and cathode.

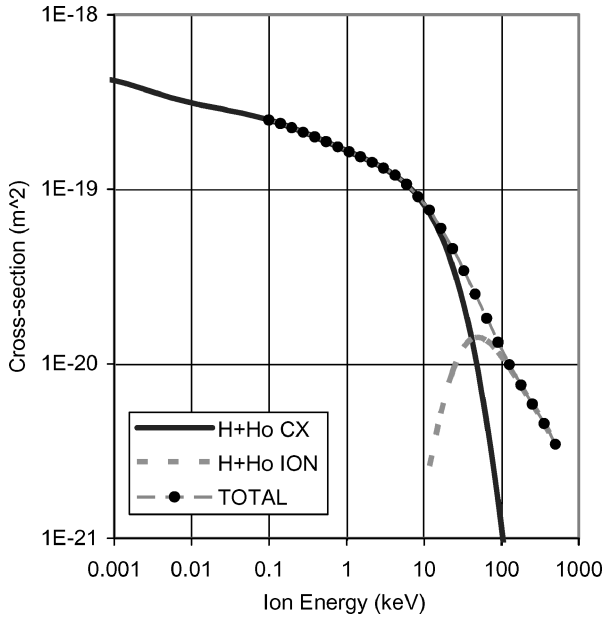

Fig. 7 Charge exchange and ionization cross sections for Hydrogen, H^+H_0 (Ref. 8).

$$v = \sqrt{\frac{2eE(x)}{m_i}} \quad E(x) = \frac{R_a R_c (E_{\text{cat}} - E_a)}{(R_a - R_c)x} + \frac{E_a R_a - E_{\text{cat}} R_c}{R_a - R_c} \tag{27}$$

The thermal velocity of the ions is assumed to be small, and the kinetic energy of the ion at the anode E_a is assumed to be equal to room-temperature thermal energy of 0.025 eV. The effect of elevated wall or grid temperatures in eventual space reactors is small and favorable, slightly reducing the atomic cross sections. Characteristic device sizes of a cathode radius of 10 cm and an anode radius of 50 cm are used. The total path-averaged cross section can be numerically integrated to obtain $\langle \sigma_a \rangle_p \approx 1 \times 10^{-19}$ m^2 for deuterium in a 50-kV well and $\langle \sigma_a \rangle_p \approx 8 \times 10^{-20}$ m^2 for deuterium in a 100-kV well.

IEC experiments to date have operated with a deuterium-deuterium reaction at fairly high pressures, ranging from 0.01 to 10 mTorr (Refs. 2 and 3) and anode radii of about 50 cm. From Eq. (26), the atomic cross sections just discussed, and typical parameters of $p = 1$ mTorr, 50-kV well, and 10-cm radii, ions make only 1.6 passes before being degraded by charge exchange and ionization. If the only limitation to the number of passes were atomic processes, one could write the reaction rate, Eq. (18), independently of confinement time by substituting Eq. (26).

$$\dot{r} = \frac{i_{\text{in-tot}}}{e} \frac{\sigma_{\text{fus}}(KE_0)}{\langle \sigma_a \rangle_p} \frac{R_{\text{cat}}}{R_a} + \frac{i_{\text{in-tot}}^2}{\pi e^2 v_{\text{core}}} \left(\frac{1}{6.436 \times 10^{22} R_a p_{\text{torr}} \langle \sigma_a \rangle_p} \right)^2 \frac{F}{R_{\text{cat}} A_c \sqrt{2\Phi}} \times \left[\frac{\langle \sigma_{\text{fus}} v \rangle}{3 v_{\text{core}}} \sqrt{N} + \frac{\sigma_{\text{fus}}(4KE_0)}{A_c \sqrt{2\Phi}} \frac{1 - (A_c/F)\sqrt{2\Phi/N}}{1 + A_c \sqrt{2\Phi/N}\,(1 - 1/F)} \right] \tag{28}$$

This equation for purely pressure-limited confinement predicts that the beam-background term is independent of pressure and linear with current. Also, the beam-beam contribution is quadratic with current and is inversely related to the square of pressure. Early results from Hirsch showed the reaction rate to increase with lower pressures, which suggested significant particle trapping in virtual anodes and cathodes.[1] However in the extensive follow-on IEC experiments to date, where the beam-background term is known to dominate the reactivity, the reaction rate is generally observed to decrease linearly with pressure,[6,12] as is similarly described by Eq. (18). Based on this model, these results suggest that the ion confinement in the experiments have not been limited by the pressure as in Eq. (26) but rather by some other process that do not allow $\#p$ to increase with lower pressures. The limiting processes are most likely ion "defocusing events," which are observed in raytracing resulting from asymmetries in the electric field caused by high-voltage grids and most importantly the stalk that supports the grid. Also, the reaction rate is observed to peak with increasing pressure and then decrease, corresponding to ions undergoing many atomic collisions before even reaching the cathode grid at higher pressure operation.

The reaction rate and expected number of passes from Eqs. (28) and (26) are shown in Figs. 8 and 9 for a proposed lab experiment with only pressure limiting the confinement, which corresponds to results of ion tracing in a three-dimensional model of the standard two-electrode system used in experiments to date. Listed in Table 2, the device parameters are chosen to represent a steady-state low-input power (500 W) device of similar dimensions to previous experiments. Conservatively, the focusing factor is chosen to be unity (no compression). Also, the acceptance is chosen to be one, meaning the beams are expanded to fill the whole circular opening in the cathode grid. For these parameters, the reaction rate is predicted to vary with pressure as shown in Fig. 8. The corresponding number of passes vs pressure is shown in Fig. 9, as calculated from Eq. (26).

Notably, in contrast to experimental data, Fig. 8 shows the independence of reaction rate on pressure at high pressures, which

Table 2 Device parameters for proposed experiment, deuterium fuel

Device parameter	Value
$i_{\text{in-tot}}$	10 mA
Cathode potential	50 kV
R_a	20 cm
R_{cat}	8 cm
N	12 beams
F	1
Acceptance, A_c	100%
Transparency, Φ	92%
v_{core}	2.19e6 m/s
σ_{fus} (50 keV)	$4.5e-31$ m^2
$\langle \sigma_a \rangle_p$	$1e-19$ m^2
σ_{fus}(200 keV)	$3.5e-30$ m^2
$\langle \sigma_{\text{fus}} v_{\text{core}} \rangle$	$5.5e-23$ m^3/s

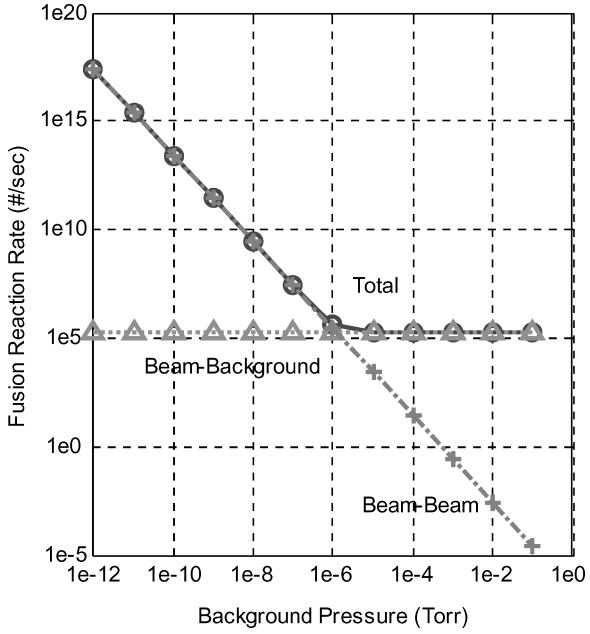

Fig. 8 Reaction rate for pressure-limited ion confinement vs device pressure.

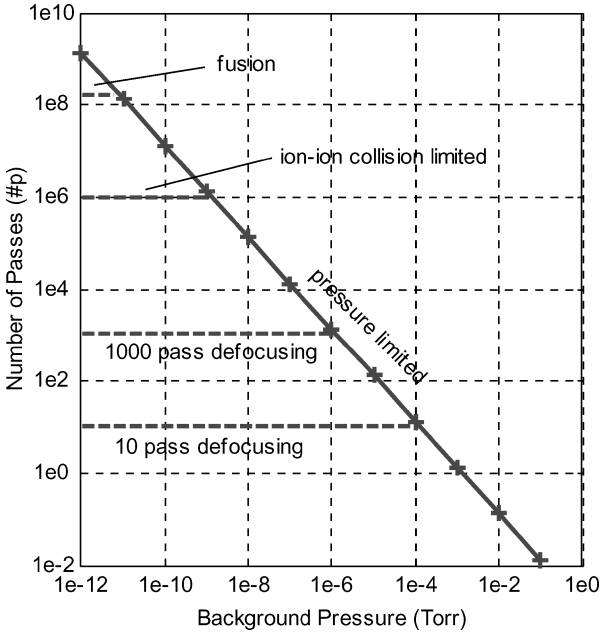

Fig. 9 Number of passes vs device pressure.

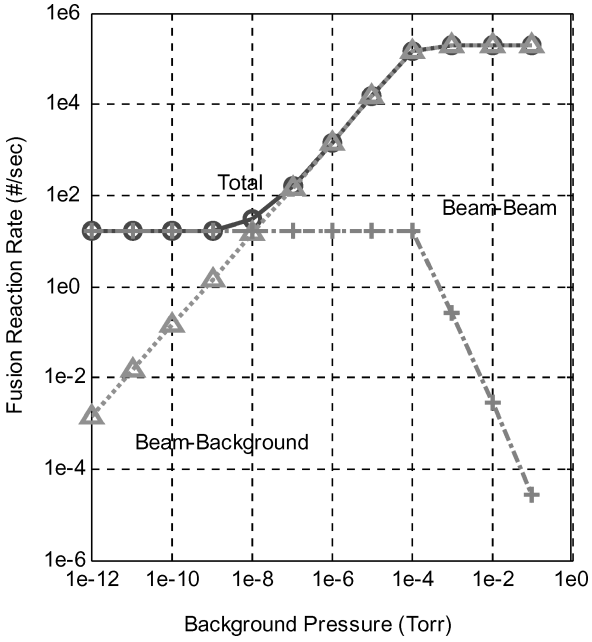

Fig. 10 Reaction rate for defocusing-limited ion confinement vs device pressure, limited to 10 passes.

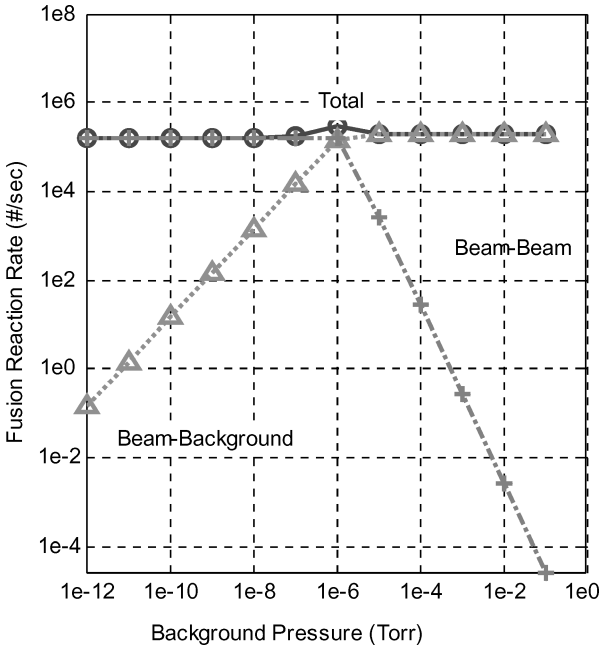

Fig. 11 Reaction rate for defocusing-limited ion confinement vs device pressure, limited to 1000 passes.

correspond to the pressures used in most previous experiments. Conversely, as the pressure is lowered beyond 10^{-6} torr, the beam-beam reactions sharply increase. This happens as the corresponding number of passes goes above 1000. However, as the confinement time increases, the assumption that the ions have little energy spread becomes less acceptable, and a more complex ion distribution should be considered.

Defocusing-Limited Ion Confinement

If for the same device the confinement is limited by ion focusing to only 10 passes, as suggested by ion particle tracing of simple one-grid cathode systems, the reaction rate varies with pressure as shown in Fig. 10. The number of passes again varies with pressure as in Fig. 9, but at lower pressures is pinned at 10. Note also the number of passes required to enter the regime where ion-ion scattering and fusion reactions will dominate, as calculated earlier.

Now at high pressure, the reaction rate is still independent of the pressure. However, as the passes begin to be limited at $\sim 10^{-4}$ torr, the rate drops off linearly with decreasing pressure. This linear relation matches experimental data, which suggests that the experiments have had confinement limited not by pressure, but by ion trajectories that are deflected by asymmetric and nonspherical grid potentials. Also, even though the beam-beam rate still eventually dominates the beam-background rate, the total rate is almost negligible and at best levels off to be independent of pressure at very low pressures. From Eq. (19), for a maximum of 10 passes the beam-beam terms are found to dominate once the pressure falls below $\sim 10^{-8}$ torr.

Improved Defocusing-Limited Ion Confinement

If the defocusing limit can be increased several orders of magnitude, the effect on the reaction-rate behavior should be easily observable in a modest experiment of similar dimension to previous efforts. Shown in Fig. 11 is the reaction rate with the defocusing limit raised to 1000 passes.

Once again, as the pressure is lowered the beam-beam terms become more important. From Eq. (19), for a maximum of 1000 passes the beam-beam terms are found to dominate once the pressure falls below $\sim 10^{-6}$ torr. In contrast to the 10-pass limited case, here the total reaction rate is relatively independent of pressure. If the current or number of passes is increased further, the rate would actually increase with decreasing pressure.

Space-Charge Limitations of Focusing Grids

The drastic increases in ion confinement from focusing grids have been predicted by ion particle tracing codes, but electrostatic lenses have limits. As the confinement time is increased, the ions create a larger and larger space charge in the beams as a result of recirculation, which eventually swamps the focusing properties of the electrostatic lenses. This limit can be estimated by equating the potential depth of the focusing lens to the potential caused by the recirculating ion beam. This represents the limit at which the lens would provide a focusing force on the beam. Although the ion path confinement is a complex function of the whole geometry, the limit for a single lens can provide a useful first-order approximation for electrostatic lenses.

Using a two-dimensional model for an infinite beam of charge, the radial field is given by Gauss' law

$$E_r = \frac{e}{\varepsilon_0 r(x)} \int_0^{r(x)} n_i(r) r \, \mathrm{d}r \tag{29}$$

Assuming a constant beam density profile,

$$\text{for} \quad r < r_g(x), \qquad E_r = \frac{e n_b r}{2\varepsilon_0}$$

$$\text{for} \quad r > r_g(x), \qquad E_r = \frac{e n_b r_g^2}{2\varepsilon_0 r(x)} \tag{30}$$

The potential profile can then be calculated, defining the potential to be zero at the grid radius, $r_{\text{g-max}}$ and integrating from the outside in,

$$V(r) = \int_{-V_{\text{g-max}}}^{V(r)} \mathrm{d}V = \int_{-r_{\text{g-max}}}^{r(x)} -E_r(r) \, \mathrm{d}r \tag{31}$$

Substituting the constant density beam electric field, Eq. (30) yields

$$\text{for} \quad r < -r_g(x), \qquad V(r) = -\frac{e n_b r_g^2}{2\varepsilon_0} \ell_n \left(-\frac{r}{r_{\text{g-max}}} \right)$$

$$\text{for} \quad 0 > r > -r_g(x), \qquad V(r) = -\frac{e n_b}{2\varepsilon_0}$$

$$\times \left[r_g^2 \ell_n \left(\frac{r}{r_{\text{g-max}}} \right) + \frac{r^2}{2} - \frac{r_g^2}{2} \right] \tag{32}$$

The voltage increases as the natural log outside the beam and is parabolic within the beam. This parabolic behavior matches well with the lens potential, which exhibits a nearly parabolic profile. Substituting in for the acceptance, the central voltage drop can be evaluated,

$$V_{\text{go}} = \frac{r_{\text{g-max}}^2 A_g^2 e n_b}{2\varepsilon_0}[1/2 - \ell_n A_g] \tag{33}$$

The bracketed term is most important when the grid acceptance is small, but is still a weak function; for $A_g = 1 \times 10^{-8}$, the term equals only ~19. Substituting for the beam density, the number of passes can be written in terms of the input current,

$$\#p = \frac{2\pi\varepsilon_0 v_g V_{\text{go}} N}{i_{\text{in-tot}}[1/2 - \ell_n A_g]} \tag{34}$$

Using the experiment parameters in Table 2, a pinching grid that would be at −40 kV and have a lens depth of $V_g = 4$ kV (modeled numerically), the number of passes is limited to 1045. This is a very rough estimate, given the complex arrangement of lens and the drift regions between focusing and defocusing regions. The next level of complexity is to model all of the lenses and the beam and to perform a self-consistent calculation to find the beam profile in such a system. This limiting mechanism forbids this simple electrostatic configuration of grids from supporting larger space charges. Although this limit might or might not prove unbreakable, it still represents a significant improvement in efficiency.

Implications for Pulsed High-Power Experiments

Recent experimental efforts have attempted to explore regimes of higher gain not by increasing confinement time, but by drastically increasing the input current using a pulsed discharge.[13] Furthermore, the existence of particle trapping in poissors in these pulsed experiments is believed to enhance the fusion reactivity. Although this analysis does not address the poissor question, the arguments about space charge buildup apply [Eq. (34)], and the space charge will act to severely defocus the ions, limiting the ion confinement to even less than what previous, steady-state defocused IECs achieved. Because of this "hidden" scaling of confinement time with input current, the reaction rates will not follow a simple power law with current. Here, the space charge is a problem because as the confinement is improved the recirculating current will increase along with the beam density. As this density becomes high enough for the beam's self-fields to internally counteract the externally imposed focusing forces, the device must transition into a more advanced mode of operation, where the space charge of the beams is somehow reduced or counteracted.

Instabilities

Because an IEC system has very small current densities as a result of the recirculation of ions along the beams, electromagnetic instabilities are avoided, leaving only electrostatic modes. The two-stream instability is present for $v/\lambda < \omega_p$, and the growth rate is a maximum at about v/λ near the limit.[14] These values do not change much in our region of interest whether considering ion-ion, ions with cold electrons, or ions with hot electrons. This means that for a given streaming velocity a minimum wavelength is required to have an unstable mode, and the mode grows approximately at the plasma frequency. For current lab devices with densities of 10^{15} m^{-3} and deuterium streaming velocities of 2×10^6 m/s, the minimum wavelength is 106 m, much bigger than the devices. For more advanced systems, say, with densities of 10^{22} m^{-3}, the minimum wavelength is only 4 cm. Although it is foreseeable that instabilities will become a problem for advanced devices, the electrostatic disturbances should not affect the predictions made by this model. Also of concern is the low-speed anode reflection region, which could possibly harbor regions of instability because the velocity drops so low there. The analysis of synchronizing, small-angle ion-ion collisions in the reflection region is an ongoing area of research in which instability might play a role.

Caveats

The main limitation for using electrostatic lenses is the buildup of space charge, which is required for a high gain system. Even if the background gas can be eliminated as a limiting mechanism, the space charge will still limit the focusing of the beams. The logical extension of increasing space charge is the Child–Langmuir limit, but the ion confinement will degrade severely before this limit is reached. The space charge counteracts the applied potentials, whether they are the main radial acceleration potentials or the secondary tangential focusing potentials. Because the focusing potentials are an order of magnitude smaller than the acceleration potential, it follows that space charge would affect the focusing potential before the main radial flow is affected greatly.

Another issue for a break-even system is the effect of ion thermalization as the confinement improves. The ion beams will heat via small-angle collisions within the counterstreaming beams and within the core region. This heating provides an additional loss mechanism for ions as the residence time of an average ion increases.

The ability to produce and maintain a neutralizing electron population in the device center is another open question. Without neutralization, the converging ion beams will tend to decelerate and defocus as a result of their space charge. If enough electrons can be provided and allowed to travel with the beams in the core region, then the ions can be made to drift through the center and possibly even be focused by the electrons. The key to maintaining this electron population with low streaming losses is to create a trap within the cathode grid. It is hypothesized that cold electrons can be produced at the low-work-function emitting grid, populate the core region, and be contained by the trapping potential. As the electrons gain energy from the ions and heat up, they can form a potential well, which could contain the thermalizing ions without letting those ions be in contact with any grids. For this to happen, though, the electron population must be in contact with the emitting grid, for which grid heating places limitations on the density and temperature of the hot electrons. A break-even reactor of reasonable dimensions and useful power levels (at least kilowatts) must be able to confine the higher densities resulting from the millions of passes a successful fusing ion must undergo. The behavior of electrons in this configuration should be a main topic of investigation and can provide a way around the space charge focusing limitations of grids.

Other concerns for a break-even IEC device include high-angle ion scattering in the core, grid heating and sputtering, and direct energy conversion with aneutronic fuels. A high-angle scattered ion from the core has a probability to directly impact a cathode grid, causing an energy loss. This reaction dominates fusion at low energy (<50 keV) and will likely set a minimum voltage for successful operation. Grid heating is a major concern and will set the dimensions of an IEC. For smaller devices, active cooling might prove too difficult, but radiatively cooled grids can handle much less heat input. Also, the sputtering of grids represents a life limiter for IECs. Because the sputter products are not in well-confined trajectories, they should quickly leave the system. The insulators will tend to be coated with these sputter products and are prone to arcing, but this could be minimized by clever design given that the sputter source locations are largely known. The possibility of using direct conversion schemes with aneutronic fuels such as D-^{3}He and p-^{11}B is promising because of the decreased system mass and increased efficiency, but drawbacks include increased complexity and higher operating voltages for these fuels.

Conclusions

The analysis of the importance of confinement on reaction rates shows that prior devices and experiments operated in a regime with limited ion confinement. This regime is characterized by a linear decrease of reaction rate with decreasing pressure and most of the fusion reactions occurring between the beams and the background gas. By enhancing the focusing properties of the grids, the ion confinement can be allowed to increase as pressure is reduced, and the reaction rate will be independent of pressure. Furthermore, keeping device parameters constant, the enhanced confinement scheme

should increase the confinement and reactivity by two orders of magnitude by increasing the confinement time at a given pressure, the most marked improvement at lower pressures.

The predicted increases in confinement and reactivity can be measured experimentally with a simple, low-cost apparatus. Experimental verification of these results will in the near term produce a much more potent, efficient inertial-electrostatic-confinement (IEC) immediately marketable as an improved portable neutron source. Applications for an inexpensive and efficient neutron source are many, including radioisotope production for medical diagnostics and therapies, industrial bulk process quality control, landmine detection, well-logging, security screening, and neutron activation analysis.[4] Improving the IEC device from the 1–10 ion passes regime up to the space charge limited regime of 1000–10,000 passes will allow the study of collective behavior in the devices. More complex collective behavior and charge-neutralizing schemes will be necessary to break the space charge-defocusing limitations of IEC devices. Only by further increasing the ion confinement can break-even operation be realized. Not only would a high-power, break-even IEC have enormous potential as a terrestrial power source, it would be a very lightweight method to harness nuclear power for fast, intrasolar system travel.

Acknowledgments

The authors would like to thank the Department of Defense NDSEG Fellowship program for partial support of this research. We would also like to acknowledge Chris Dobson at NASA Marshall Space Flight Center for his assistance and experience, as well as our colleagues at the Massachusetts Institute of Technology Space Systems Lab for a variety of discussions and input.

References

[1]Hirsch, R. L., "Inertial Electrostatic Confinement of Ionized Fusion Gases," *Journal of Applied Physics*, Vol. 38, No. 11, 1967, pp. 4522–4534.

[2]Hirsch, R. L., "Experimental Studies of a Deep, Negative, Electrostatic Potential Well in Spherical Geometry," *Physics of Fluids*, Vol. 11, No. 11, 1968, pp. 2486–2490.

[3]Miley, G. H., Gu, Y., DeMora, J. M., Stubbers, R. A., Hochberg, T. A., Nadler, J. H., and Anderl, R. A., "Discharge Chararcteristics of the Spherical Inertial Electrostatic Confinement (IEC) Device," *IEEE Transactions on Plasma Science*, Vol. 25, No. 4, 1997, pp. 733–739.

[4]Kulcinski, G. L., Ashley, R. P., McMahon, P. B., Breum, R. A., Santarius, J. F., and Schmitt, H. H., "Demonstration of D^3He Fusion in an Inertial Electrostatic Confinement Device," Progress Report, Fusion Technology Inst., Univ. of Wisconsin, 29 Jan. 1998–28 Jan. 1999.

[5]Bussard, R. W., "Some Physics Considerations of Magnetic Inertial-Electrostatic Confinement: a New Concept for Spherical Converging-Flow Fusion," *Fusion Technology*, Vol. 19, March 1991, pp. 273–293.

[6]Gu, Yibin, "Experimental Study of Proton Rate Density in a Spherical Inertial Electrostatic Confinement Fusion Device," Ph.D. Dissertation, Electrical Engineering, Univ. of Illinois at Urbana Champaign, 1998.

[7]Moses, R., "Enhancing IEC Performance with Focusing Grids," presented at the Phys. Spherical Continuous Inertial Fusion Workshop, LANL, Jan. 1995.

[8]International Atomic Energy Agency, Atomic cross-sections physics database, *The International Atomic Energy Agency—Atomic and Molecular Data Information System ALLADIN*, collisional database, *URL: http://www-amdis.iaea.org/aladdin.html* (Dataset: ORNL-CFADC, 1990-01-06).

[9]Huba, J. D., *NRL Plasma Formulary*, Naval Research Lab., Washington, DC, 1994, pp. 44–55.

[10]Farnsworth, P., "Electric Discharge Device for Producing Interactions Between Nuclei," U.S. Patent 3 258 402, 28 June 1966.

[11]Ashley, R. P., Kulcinski, G. L., Santarius, J. F., Karupakar Murali, S., Piefer, G., and Radel, R., "Steady-State D-^{3}He Proton Production in an IEC Fusion Device," *14th Topical Meeting on the Technology of Fusion Energy*, Park City, Utah, Oct. 2000.

[12]Thorson, T. A., Durst, R. D., Fonck, R. J., and Sontag, A. C., "Fusion Reactivity Characterization of a Spherically-Convergent Ion Focus," *Nuclear Fusion*, Vol. 38, No. 4, 1998, pp. 495–507.

[13]Nadler, J. H., and Miley, G. H., "A Breakeven Fusion Power Unit for Space Applications," Final Report NASA SBIR Contract #NAS8-99044, NPL Associates, Champaign, IL, June 1999.

[14]Chen, F. F., *Introduction to Plasma Physics and Controlled Fusion, Volume 1: Plasma Physics*, Plenum Press, New York, 1984.